ACADEMIC PRESS

Available online at www.sciencedirect.com

SCIENCE DIRECT®

Journal of Solid State Chemistry 170 (2003) 82–93

JOURNAL OF SOLID STATE CHEMISTRY

http://elsevier.com/locate/jssc

Diffusion of hydrogen isotopes and their mutual perturbation in $Ti_{0.33}V_{0.67}H_xD_y$ ($x+y\approx0.9$) studied by ^1H and ^2H NMR

Shigenobu Hayashi*

Institute for Materials and Chemical Process, National Institute of Advanced Industrial Science and Technology (AIST), Tsukuba Central 5, 1-1-1 Higashi, Tsukuba, Ibaraki 305-8565, Japan

Received 28 March 2002; received in revised form 20 June 2002; accepted 27 August 2002

Abstract

$Ti_{0.33}V_{0.67}H_xD_y$ ($x+y\approx0.9$) alloys have been studied by means of X-ray powder diffraction (XRD), differential scanning calorimetry (DSC) and ^1H and ^2H NMR. The crystal structures are body-centered-cubic (bcc) dominantly, being mixed with a face-centered-cubic (fcc) phase. A phase transition similar to that from the δ_D phase to the α_D phase in the V–D system is observed in all the samples except for the protide. H and D are considered to occupy tetrahedral sites. The temperature and frequency dependence of spin-lattice relaxation times T_1 of ^1H and ^2H has been analyzed by Bloembergen–Purcell–Pound equations with a distribution of correlation times, and parameters of hydrogen diffusion are estimated. The mean activation energy for D diffusion (E_D) is higher than that for H diffusion (E_H). E_H is constant while E_D increases slightly with the [D]/[H] ratio. The distribution of the correlation times increases as the [D]/[H] ratio decreases.

Keywords: Hydrogen-absorbing material; Alloy; Metal hydride; Diffusion; Isotope effect; Nuclear magnetic resonances; NMR

1. Introduction

Metal hydrides are attractive as hydrogen-storage materials. Titanium–vanadium alloys form stable hydrides as well as Ti and V metals do [1,2]. The Ti–V–H system is expected to be synthesized at any [Ti]/[V] ratio, since the Ti–V alloy forms a solid solution with a body-centered-cubic (bcc) structure over wide ranges of composition and temperature [3]. The crystal structure of monoprotide $Ti_{1-z}V_zH_x$ ($x\approx1$) depends on the [Ti]/[V] ratio. (In order to avoid confusion, the following nomenclatures are used in this work; protium for H, deuterium for D, hydrogen for both H and D, protide for metal—H, deuteride for metal—D and hydride for both metal—H and metal—D.) The structure is bcc in the range $0.2\leqslant z\leqslant0.8$ [4], while it is body-centered-tetragonal (bct) for $0.9\leqslant z\leqslant1.0$ [2,5]. On the other hand, the monodeuteride $Ti_{1-z}V_zD_x$ ($x\approx1$) has always the bcc structure [6,7]. Our inelastic neutron scattering study on $Ti_{1-z}V_zH_x$ ($0.2\leqslant z\leqslant0.9$, $x\approx1$) has revealed that the site occupancy depends on the [Ti]/[V] ratio [5]. Octahedral (O) sites are dominantly occupied in the V-rich alloys, whereas tetrahedral (T) sites are occupied in the Ti-rich alloys. In the extreme case of pure vanadium, the structures and the phase diagrams of hydrides have been extensively studied in the past [8]. It is known that H and D occupy the O and T sites, respectively, in the monohydride phase of vanadium, leading to the bct and bcc structures, respectively. In contrast to the monoprotide, the structure of diprotide $Ti_{1-z}V_zH_2$ is face-centered-cubic (fcc) for $0\leqslant z\leqslant1$ [9].

In the previous works we have studied hydrogen diffusion in the Ti–V–H(D) system by means of ^1H and ^2H NMR [6,10–12]. The apparent activation energy decreases in the V-rich alloys. The activation energy of D diffusion is larger than that of H diffusion at a given alloy composition.

As described above, the crystal structure of the monoprotide $Ti_{1-z}V_zH_x$ ($x\approx1$) changes from bcc to bct within the range $0.8<z<0.9$, while the monodeuteride $Ti_{1-z}V_zD_x$ ($x\approx1$) has always the bcc structure. When both H and D are contained simultaneously, there may be a structural boundary or an intermediate region around $0.8<z<0.9$ only in the H-rich region. We studied V–H–D systems with the ([H]+[D])/[V] ratio

*Fax: +81-298-61-4515.
E-mail address: hayashi.s@aist.go.jp (S. Hayashi).

0022-4596/03/$ - see front matter © 2002 Elsevier Science (USA). All rights reserved.
PII: S0022-4596(02)00026-9

of 0.8 by means of NMR, and found that the site occupancy, the diffusions of H and D, and furthermore the crystal structure depend on the [D]/[H] ratio [7]. We studied the $Ti_{0.1}V_{0.9}H_xD_y$ ($x+y\approx0.7$) systems also by NMR [13,14]. The systems have features similar to those in the V–H–D systems, although Ti addition shows some effects on the site occupancies and hydrogen diffusion.

In the present work, we have studied $Ti_{0.33}V_{0.67}$–H–D systems. This system is suitable to study isotope effects in hydrogen diffusion, since the crystal structures of the monoprotide $Ti_{0.33}V_{0.67}H_x$ ($x\approx1$) and monodeuteride $Ti_{0.33}V_{0.67}D_x$ ($x\approx1$) are both bcc. The diffusion is expected to depend on the [D]/[H] ratio, and the mutual perturbation between H and D can be extracted. We report the results of X-ray powder diffraction (XRD), differential scanning calorimetry (DSC) and ^{1}H and ^{2}H NMR. The temperature and frequency dependence of the spin-lattice relaxation times are analyzed by considering a distribution of the correlation time.

2. Experimental

2.1. Materials

A block of the $Ti_{0.33}V_{0.67}$ alloy was supplied by the Central Research Laboratory of Mitsubishi Metal Corporation. The primary hydrogenation was carried out in a stainless-steel reactor under a high H_2 or D_2 pressure, resulting in $Ti_{0.33}V_{0.67}H_{1.55}$ and $Ti_{0.33}V_{0.67}H_{0.12}D_{1.67}$. The latter contained a small amount of H, which was probably due to H_2 or HD in the D_2 gas used. The purity of the D_2 gas was 99.5%. These samples were partially outgassed at elevated temperatures in a glass vacuum line to obtain parent monohydride samples, which were $Ti_{0.33}V_{0.67}H_{0.90}$ and $Ti_{0.33}V_{0.67}H_{0.07}D_{0.88}$. The alloys containing both H and D, $Ti_{0.33}V_{0.67}H_xD_y$, were prepared by mixing two parent samples in required ratios and then homogenizing the mixture inside a closed chamber at 700 K for a week. After the subsequent slow cooling, all evolved gas components were reabsorbed. Thus, we prepared the samples $Ti_{0.33}V_{0.67}H_{0.63}D_{0.29}$, $Ti_{0.33}V_{0.67}H_{0.49}D_{0.43}$ and $Ti_{0.33}V_{0.67}H_{0.35}D_{0.58}$. The H and D contents of those samples were determined with a combined apparatus of thermogravimetry and mass spectrometry, the detail of which was reported elsewhere [15]. The errors of the contents were about $\pm5\%$ of the quoted figure.

2.2. X-ray diffraction and thermal analysis

X-ray powder diffraction patterns were measured by a Rigaku MiniFlex diffractometer with Cu$K\alpha$ radiation at room temperature. DSC measurements were carried out in the temperature range between 120 and 295 K using a Rigaku Thermoflex DSC8230 combined with a Rigaku thermal analysis station TAS100. The sample temperature was raised at a rate of 5 K/min.

2.3. NMR measurements

NMR measurements were similar to those in our previous works [7,13,14]. ^{1}H NMR was measured by a Bruker CXP90 spectrometer equipped with a Tecmag Real-time NMR Station MiniMacSpect operated by MacNMR5.4 software and by a Bruker ASX400 spectrometer. Larmor frequencies were set at 31.6 ± 1.2 and 60.0 ± 0.3 MHz for the former and at 400.13 MHz for the latter. Although the stability of the electromagnet of CXP90 was not very good, the drift of the magnetic field in each experiment was neglected when compared to the line width of the signal. The 90° pulse widths were 1.9–4.0 μs at 31.6 MHz, 1.4–2.0 μs at 60.0 MHz and 3.9–5.9 μs at 400.13 MHz. The ^{2}H NMR measurements were performed by Bruker ASX200 and MSL400 spectrometers. Larmor frequencies were 30.7 and 61.4 MHz for ASX200 and MSL400, respectively. The 90° pulse widths were 3.5–3.6 μs at 30.7 MHz and 3.2–5.8 μs at 61.4 MHz.

The inversion recovery pulse sequence followed by the quadrupole (or solid) echo pulse sequence ($180^\circ-\tau-90_x{}^\circ-\tau_1-90_y{}^\circ-\tau_2-$echo) was used for most of the T_1 measurements. For the T_1 measurements at 77 K, the magnetization was first saturated by a string of near 90° pulses, and then its recovery with time was monitored. The pulse sequence was $(90^\circ-\tau_3)_n-\tau-90_x{}^\circ-\tau_1-90_y{}^\circ-\tau_2-$echo. In those pulse sequences, τ denotes the variable delay time and τ_1, τ_2 and τ_3 are fixed delay times. The ^{1}H and ^{2}H NMR spectra presented in this work were extracted from the data of the T_1 measurements by selecting the spectra with the longest τ value.

3. Results and discussion

3.1. X-ray powder diffraction

Fig. 1 shows X-ray powder diffraction patterns. The patterns can be interpreted as consisting of two structures, bcc and fcc, although the relatively broad peaks suggest a distribution of lattice constants and/or a distortion. The two structures are ascribed to monohydride (β) and dihydride (γ) phases, respectively. The strongest peak in bcc is the (110) peak at $2\theta=40^\circ$, while that in fcc is the (111) peak at 35°. The (200) peak in fcc (at 41°) overlaps with the tail of the (110) peak in bcc. The (200) peak in bcc and the (220) peak in fcc overlap partly with each other in the range of 55–60°, whereas the (211) peak in bcc and the (311) and (222) peaks in fcc overlap similarly in the range of 70–75°. The observed patterns indicate that the bcc phase is dominant. The

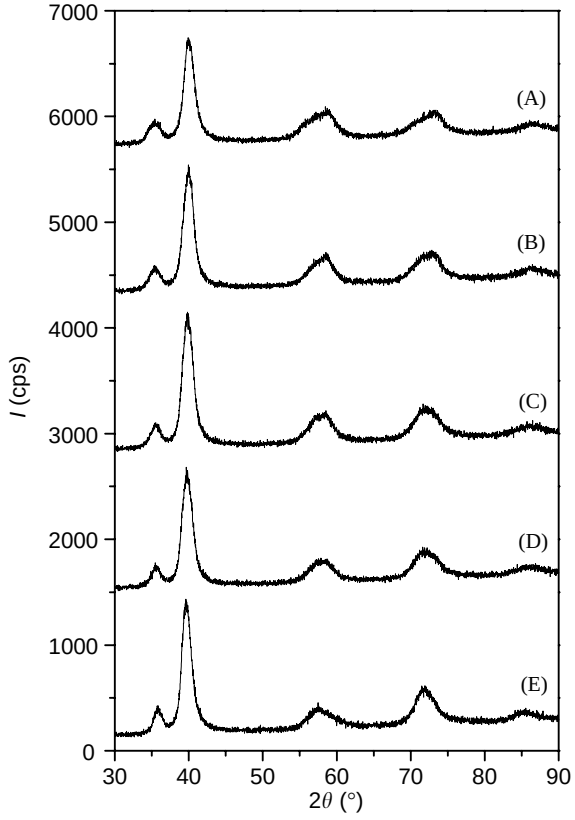

Fig. 1. X-ray powder diffraction patterns of (A) $Ti_{0.33}V_{0.67}H_{0.90}$, (B) $Ti_{0.33}V_{0.67}H_{0.63}D_{0.29}$, (C) $Ti_{0.33}V_{0.67}H_{0.49}D_{0.43}$, (D) $Ti_{0.33}V_{0.67}H_{0.35}D_{0.58}$ and (E) $Ti_{0.33}V_{0.67}H_{0.07}D_{0.88}$ at room temperature. The zero line of the pattern is shifted arbitrarily.

Table 1
Crystal structures

Sample	a_0 (nm) of bcc[a]	a_0 (nm) of fcc[b]
$Ti_{0.33}V_{0.67}H_{0.90}$	0.318	0.440
$Ti_{0.33}V_{0.67}H_{0.63}D_{0.29}$	0.319	0.440
$Ti_{0.33}V_{0.67}H_{0.49}D_{0.43}$	0.320	0.438
$Ti_{0.33}V_{0.67}H_{0.35}D_{0.58}$	0.320	0.438
$Ti_{0.33}V_{0.67}H_{0.07}D_{0.88}$	0.321	0.435
$Ti_{0.33}V_{0.67}H_{1.55}$	0.319	0.431
$Ti_{0.33}V_{0.67}H_{0.12}D_{1.67}$	ND[c]	0.431

[a] The error is ± 0.002.
[b] The error is ± 0.001.
[c] ND: not detected.

fraction of bcc is roughly 85% in metal base. Hydrogen is considered to occupy the T sites. The mean lattice constants of the two phases are listed in Table 1, together with the values of the dihydride samples.

With increase in the D fraction, the lattice constant in bcc increases slightly whereas that in fcc decreases. The values of the dihydride samples suggest that there is no isotope effect in the lattice constant. On the other hand, the lattice constants are dependent on the [Ti]/[V] ratio [4]. The lattice constants in fcc are 0.428 nm for vanadium diprotide and 0.446 nm for titanium diprotide [16]. The value of the Ti–V diprotide depends on the [Ti]/[V] ratio linearly [4,9]. The similar relation was also obtained in the monoprotide [4]. The [Ti]/[V] ratio might be different between the bcc and fcc phases. Ti is more condensed in the fcc phase than in the bcc phase. The deuteride sample has the most homogeneous metal distribution among five monohydride samples. With increase in the H fraction Ti is more condensed in the fcc phase.

3.2. DSC

Fig. 2 shows the results of the DSC measurements, and the numerical results are summarized in Table 2. An endothermic peak is observed except for the protide sample. The peak intensity is much smaller than those in VH_xD_y and $Ti_{0.1}V_{0.9}H_xD_y$ [7,13]. With increase in the H fraction, the peak shifts towards the lower temperature. The endothermic peak is ascribed to the order–disorder

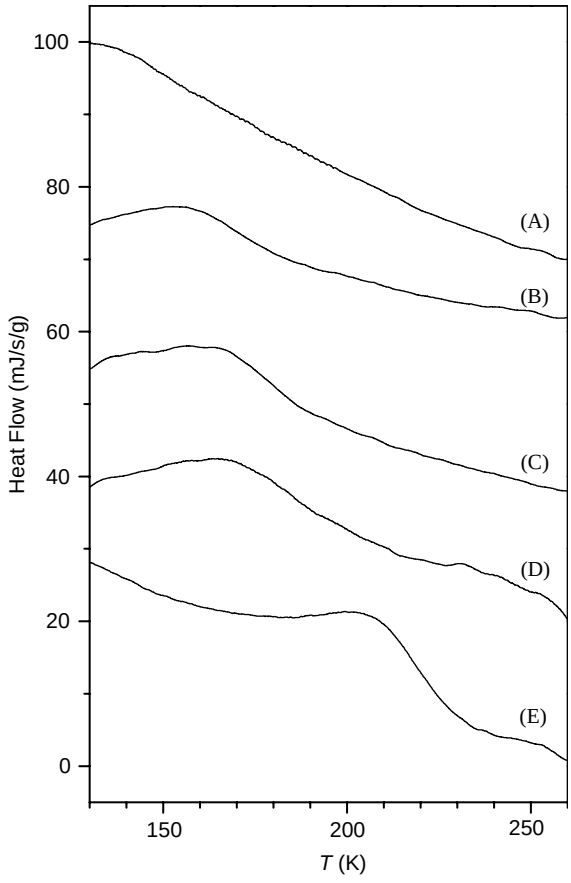

Fig. 2. DSC curves of (A) $Ti_{0.33}V_{0.67}H_{0.90}$, (B) $Ti_{0.33}V_{0.67}H_{0.63}D_{0.29}$, (C) $Ti_{0.33}V_{0.67}H_{0.49}D_{0.43}$, (D) $Ti_{0.33}V_{0.67}H_{0.35}D_{0.58}$ and (E) $Ti_{0.33}V_{0.67}H_{0.07}D_{0.88}$. Heat absorption is expressed as the positive direction. The magnitudes of the heat flow are normalized by the sample weight, and the zero positions are shifted by arbitrarily amounts.

Table 2
Results of DSC measurements

Sample	T_L[a] (K)	T_M[b] (K)	T_H[c] (K)
$Ti_{0.33}V_{0.67}H_{0.90}$	ND[d]	ND[d]	ND[d]
$Ti_{0.33}V_{0.67}H_{0.63}D_{0.29}$	<115	155	185
$Ti_{0.33}V_{0.67}H_{0.49}D_{0.43}$	<135	165	190
$Ti_{0.33}V_{0.67}H_{0.35}D_{0.58}$	140	170	215
$Ti_{0.33}V_{0.67}H_{0.07}D_{0.88}$	150	205	235

[a] Lower temperature end within an error of ±5 K.
[b] Temperature of the maximum point within an error of ±5 K.
[c] Higher temperature end within an error of ±5 K.
[d] ND: not detected.

transition of the D sublattice by analogy with the V–D system [8]. D occupies the tetrahedral (T) site and tends to be ordered. H and Ti introduce disorder and hinder the D ordering.

3.3. ^1H NMR spectra

^{1}H NMR spectra have been measured at 77 K and in the temperature range between 140 and 400 K. Fig. 3 shows spectra measured at 77 K. At 77 K ^{1}H spins are expected to be in a rigid lattice state. The line width is determined by dipole–dipole interactions between ^{1}H and ^{51}V and between ^{1}H and ^{1}H. Contributions of ^{47}Ti and ^{49}Ti are neglected, since their natural abundances are only 7.3% and 5.5% and their nuclear dipole moments are about $\frac{1}{5}$ of ^{51}V. Contribution of ^{2}H is also neglected because its dipole moment is 1/6.51 of ^{1}H. The full-width at half-maximum (FWHM) at 77 K are in the following order, $Ti_{0.33}V_{0.67}H_{0.90}$ (55 kHz) > $Ti_{0.33}V_{0.67}H_{0.63}D_{0.29}$ (48 kHz) > $Ti_{0.33}V_{0.67}H_{0.49}D_{0.43}$ (42 kHz) > $Ti_{0.33}V_{0.67}H_{0.35}D_{0.58}$ (29 kHz), which is reasonable because the magnitude of ^{1}H–^{1}H interaction decreases with decrease in the H fraction. The second moments are 590, 490, 420 and 320 kHz^2 for the above samples, respectively. The former three values are estimated by fitting a Gaussian line shape to the observed spectra, where the experimental errors are about ±10%. On the other hand, the last one is calculated directly from the digital data of the spectrum because the line shape deviates from characteristic line shapes such as Gaussian, Lorentzian and their mixed ones. Therefore, the error might be more than ±20%.

Fig. 4 shows temperature dependence of the spectra of $Ti_{0.33}V_{0.67}H_{0.63}D_{0.29}$ measured at 60.0 MHz and other samples show similar temperature dependence of the line shape. Fig. 5 shows temperature dependence of the line width. Motional narrowing starts above 77 K and finishes at about 200 K. The temperature range depends on the sample, which is in the order that $Ti_{0.33}V_{0.67}H_{0.90}$ < $Ti_{0.33}V_{0.67}H_{0.63}D_{0.29}$ < $Ti_{0.33}V_{0.67}H_{0.49}D_{0.43}$ < $Ti_{0.33}V_{0.67}H_{0.35}D_{0.58}$. This order might reflect hydrogen mobility. In the intermediate temperature range of the motional narrowing, the line shape seems to consist of two components, a broad Gaussian and a narrow Lorentzian component. The two-component nature of the line shape becomes weak as the D fraction increases.

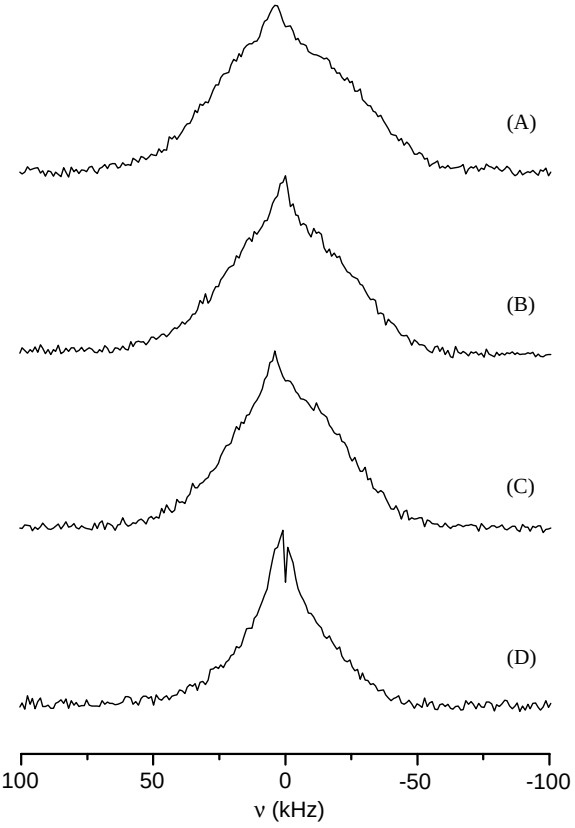

Fig. 3. ^{1}H NMR spectra of (A) $Ti_{0.33}V_{0.67}H_{0.90}$, (B) $Ti_{0.33}V_{0.67}H_{0.63}D_{0.29}$, (C) $Ti_{0.33}V_{0.67}H_{0.49}D_{0.43}$ and (D) $Ti_{0.33}V_{0.67}H_{0.35}D_{0.58}$, measured at 60.0 MHz and 77 K.

After the motional narrowing finishes there is still a broad component at the bottom in the low-frequency side. This component is ascribed to the fcc phase, and is observed in $Ti_{0.33}V_{0.67}H_{0.90}$ and $Ti_{0.33}V_{0.67}H_{0.63}D_{0.29}$.

3.4. ^1H spin-lattice relaxation time

^{1}H spin-lattice relaxation times have been measured at 77 K and in the temperature range between 140 and 400 K. The experimentally obtained T_1 values are plotted as a function of inverse temperature in Figs. 6–9. The recovery of the ^{1}H magnetization is exponential in all the samples at the three Larmor frequencies. The experimental error of each T_1 value is ±5% or less in most cases.

At 77 K and 60.0 MHz, the ^{1}H T_1 values are 0.87±0.08, 0.96±0.09 and 1.06±0.09 s for $Ti_{0.33}V_{0.67}H_{0.90}$, $Ti_{0.33}V_{0.67}H_{0.63}D_{0.29}$ and $Ti_{0.33}V_{0.67}H_{0.49}D_{0.43}$, respectively. We could not get a reliable value for $Ti_{0.33}V_{0.67}H_{0.35}D_{0.58}$ at 77 K because of low signal-to-noise ratios. The T_1 values at 140 K and 400.13 MHz are

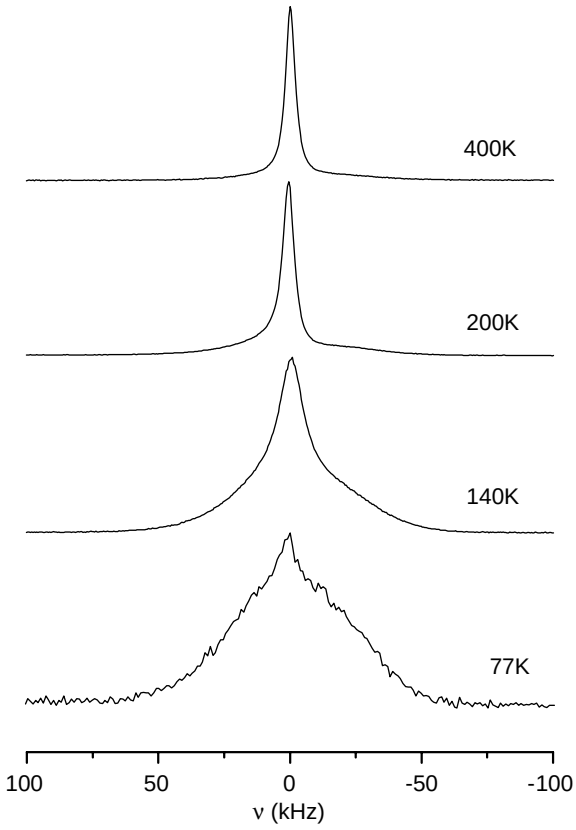

Fig. 4. Temperature dependence of ^{1}H NMR spectra of $Ti_{0.33}V_{0.67}H_{0.63}D_{0.29}$ at 60.0 MHz.

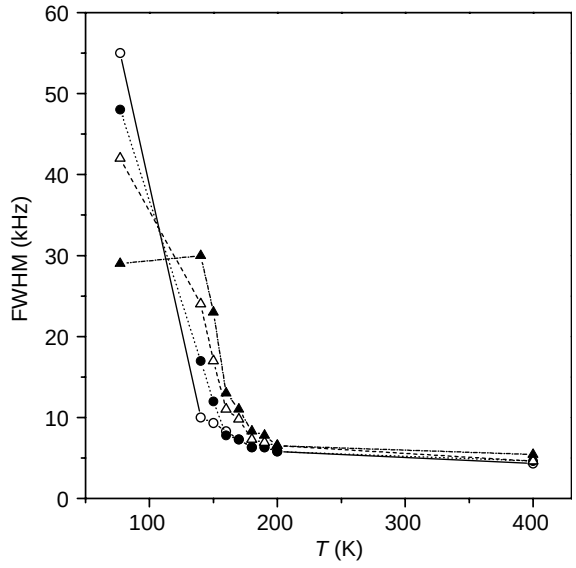

Fig. 5. FWHM of ^{1}H NMR signal at 60.0 MHz in (○) $Ti_{0.33}V_{0.67}H_{0.90}$, (●) $Ti_{0.33}V_{0.67}H_{0.63}D_{0.29}$, (△) $Ti_{0.33}V_{0.67}H_{0.49}D_{0.43}$ and (▲) $Ti_{0.33}V_{0.67}H_{0.35}D_{0.58}$.

0.47, 0.54, 0.50 and 0.56 s for $Ti_{0.33}V_{0.67}H_{0.90}$, $Ti_{0.33}V_{0.67}H_{0.63}D_{0.29}$, $Ti_{0.33}V_{0.67}H_{0.49}D_{0.43}$ and $Ti_{0.33}V_{0.67}H_{0.35}D_{0.58}$, respectively. Their errors are ± 0.02 s. Korringa constants $T_{1e}T$ of $Ti_{0.33}V_{0.67}H_{0.90}$, $Ti_{0.33}V_{0.67}H_{0.63}D_{0.29}$ and $Ti_{0.33}V_{0.67}H_{0.49}D_{0.43}$ are estimated from the T_1 values at 77 K and 60.0 MHz, while it is estimated from the T_1 values at 140 K and 400.13 MHz for $Ti_{0.33}V_{0.67}H_{0.35}D_{0.58}$. Those values are listed in Table 3.

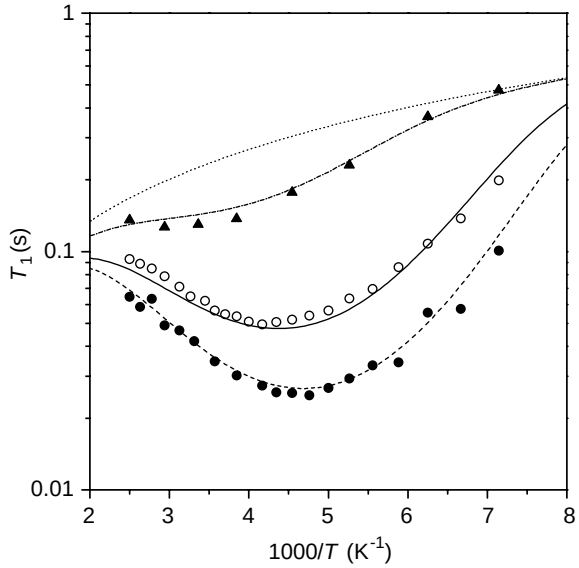

Fig. 6. ^{1}H spin-lattice relaxation times in $Ti_{0.33}V_{0.67}H_{0.90}$ at 31.6 (●), 60.0 (○) and 400.13 MHz (▲), and their simulated results indicated by the chain, solid and chain-dotted lines, respectively. The dotted line indicates the contribution of conduction electrons.

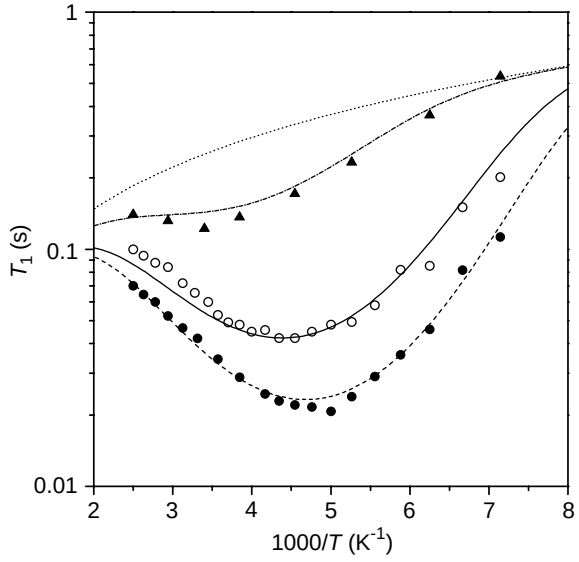

Fig. 7. ^{1}H spin-lattice relaxation times in $Ti_{0.33}V_{0.67}H_{0.63}D_{0.29}$ at 31.6 (●), 60.0 (○) and 400.13 MHz (▲), and their simulated results indicated by the chain, solid and chain-dotted lines, respectively. The dotted line indicates the contribution of conduction electrons.

As are shown in Figs. 6–9, T_1 yields a minimum at about 210 K at 31.6 MHz. As the measuring frequency increases, the minimum position shifts towards the

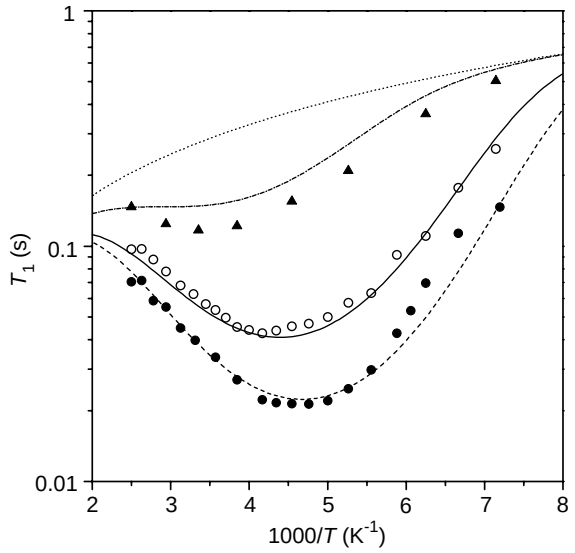

Fig. 8. ^{1}H spin-lattice relaxation times in $Ti_{0.33}V_{0.67}H_{0.49}D_{0.43}$ at 31.6 (●), 60.0 (○) and 400.13 MHz (▲), and their simulated results indicated by the chain, solid and chain-dotted lines, respectively. The dotted line indicates the contribution of conduction electrons.

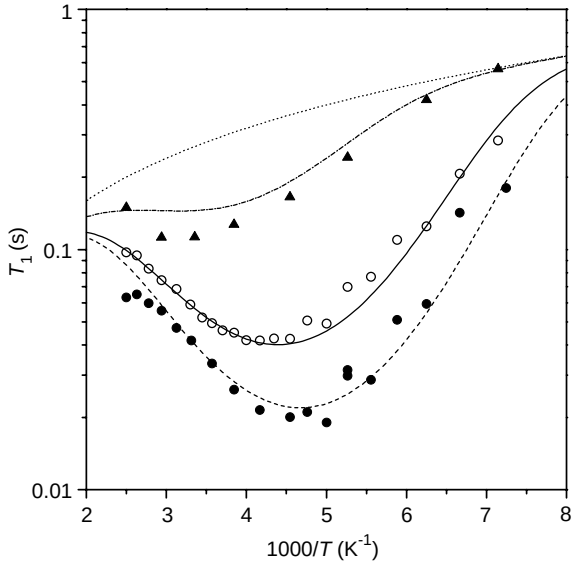

Fig. 9. ^{1}H spin-lattice relaxation times in $Ti_{0.33}V_{0.67}H_{0.35}D_{0.58}$ at 31.6 (●), 60.0 (○) and 400.13 MHz (▲), and their simulated results indicated by the chain, solid and chain-dotted lines, respectively. The dotted line indicates the contribution of conduction electrons.

higher temperature and the minimum value increases. Effect of the phase transition is negligible.

3.5. Analysis of ^{1}H spin-lattice relaxation time

As has been analyzed in the previous work [7,13,14], the ^{1}H spin-lattice relaxation rate can be expressed as

$$(T_1)^{-1} = (T_{1d})^{-1} + (T_{1e})^{-1} + (T_{1p})^{-1}, \quad (1)$$

where $(T_{1d})^{-1}$ is contribution from modulation of nuclear dipolar interactions, $(T_{1e})^{-1}$ arises from fluctuation of hyperfine interaction between the nuclear spin and conduction electrons, and $(T_{1p})^{-1}$ is contribution from the dipolar interaction between the nuclear spin and electron spins on paramagnetic impurities. The temperature dependence of T_{1e} is given by Korringa relation, $T_{1e}T$ =constant. The Korringa constants in Table 3 are intermediate between those of titanium hydride and vanadium hydride [11], which indicates that the contribution of paramagnetic impurities is negligible in the samples of this work.

According to Bloembergen, Purcell and Pound (BPP) [17], the dipolar contribution in Eq. (1) is written as

$$\begin{aligned}(T_{1d})^{-1} &= \frac{2}{3}M_{HH}\left[\frac{0.5\tau_H}{1+(0.5\omega_H\tau_H)^2}+\frac{2\tau_H}{1+(\omega_H\tau_H)^2}\right] \\ &\quad + M_{HV}\left[\frac{0.5\tau_H}{1+\{(1-\gamma_V/\gamma_H)\omega_H\tau_H\}^2}\right. \\ &\quad \left.+\frac{1.5\tau_H}{1+(\omega_H\tau_H)^2}+\frac{3\tau_H}{1+\{(1+\gamma_V/\gamma_H)\omega_H\tau_H\}^2}\right]. \quad (2)\end{aligned}$$

In the above equation M_{HH} and M_{HV} are second moments given by

$$M_{HH} = \frac{3}{5}\gamma_H^4\hbar^2 I_H(I_H+1)\sum_i r_i^{-6} \quad (3)$$

and

$$M_{HV} = \frac{4}{15}\gamma_H^2\gamma_V^2\hbar^2 I_V(I_V+1)\sum_j r_j^{-6}, \quad (4)$$

where ω_H is an angular resonance frequency of ^{1}H, γ_H and γ_V are gyromagnetic ratios of ^{1}H and ^{51}V spins, respectively, $\hbar$ is Planck's constant, and r_i and r_j are distances between ^{1}H spins and between ^{1}H and ^{51}V spins, respectively. I_H and I_V are nuclear spin quantum numbers of ^{1}H and ^{51}V spins, which are 1/2 and 7/2, respectively. A mean residence time of H is denoted as τ_H. Because only H is mobile, correlation times between ^{1}H spins and between ^{1}H and ^{51}V spins are $\tau_{HH} = 0.5\tau_H$ and $\tau_{HV} = \tau_H$, respectively. For a thermally activated diffusion process, τ_H follows Arrhenius relation, $\tau_H = \tau_{0H}\exp(E_H/RT)$, where τ_{0H} is a mean residence time at the infinite temperature or the inverse of a frequency factor, E_H is an activation energy, and R is a gas constant.

The BPP equation predicts that the plot of $\log T_{1d}$ vs. the inverse of temperature has a minimum, where $\omega_H\tau_H \cong 1$, and that it is symmetric with respect to the minimum position. Moreover, these equations also predict ω_H^2 dependence of T_{1d} at low temperatures where $\omega_H\tau_H \gg 1$. At high temperatures where $\omega_H\tau_H \ll 1$,

Table 3
^{1}H Korringa constants and parameters of H diffusion

Sample	$T_{1e}T$[a] (s K)	Site	τ_{0H}[b] (s)	E_H[c] (kJ/mol)	β_Q[d] (kJ/mol)	β_0[e]	f_1[f]
$Ti_{0.33}V_{0.67}H_{0.90}$	67±6	T	3×10^{-14}	21.3	0	4.3	0.35
$Ti_{0.33}V_{0.67}H_{0.63}D_{0.29}$	74±7	T	3×10^{-14}	21.3	0	4.0	0.45
$Ti_{0.33}V_{0.67}H_{0.49}D_{0.43}$	82±7	T	3×10^{-14}	21.3	0	3.8	0.48
$Ti_{0.33}V_{0.67}H_{0.35}D_{0.58}$	78±3	T	3×10^{-14}	21.3	0	3.5	0.48

[a] Korringa constant.
[b] Assumed.
[c] The error is about ±0.5.
[d] The error is about ±2.
[e] The error is about ±0.2.
[f] The error is about ±0.03.

the T_{1d} value is independent of ω_H, or the applied magnetic field.

In the previous works on VH_xD_y and $Ti_{0.1}V_{0.9}H_xD_y$ the T_{1d} curves are asymmetric with respect to the minimum position, and there is a pronounced deviation from the low-temperature ω_H^2 proportionality [7, 13, 14]. The modified BPP equation was used, in which suitable parameters were introduced to adjust the temperature and frequency dependences of T_{1d} [18–20].

In contrast to the above empirical approach, another approach is to assume an asymmetric distribution of mean residence times rather than a sharp value of τ_H [21]. The above procedure was followed to describe the H dynamics in β-$Ti_{1-y}V_yH_x$ [12], which might possess a distribution of non-equivalent positions and potential barriers for the diffusing particles. In the present work, we apply the last approach since the adjustable parameters have some physical meanings. The relaxation rate is

$$(T_{1d})^{-1} = \int F(S)\left\{\frac{2}{3}M_{HH}\left[\frac{0.5\tau_H}{1+(0.5\omega_H\tau_H)^2}+\frac{2\tau_H}{1+(\omega_H\tau_H)^2}\right] + f_1 M_{HV}\left[\frac{0.5\tau_H}{1+\{(1-\gamma_V/\gamma_H)\omega_H\tau_H\}^2} + \frac{1.5\tau_H}{1+(\omega_H\tau_H)^2}+\frac{3\tau_H}{1+\{(1+\gamma_V/\gamma_H)\omega_H\tau_H\}^2}\right]\right\} dS, \quad (5)$$

where $F(S)$ is a distribution function,

$$F(S) = \frac{1}{\beta_1\sqrt{\pi}}\exp\left(-\frac{S^2}{\beta_1^2}\right), \quad (6)$$

$$S = \ln\frac{\tau_H}{\tau_{mH}}, \quad (7)$$

$$\beta_1^2 = \beta_0^2 + \left(\frac{\beta_Q}{RT}\right)^2 \quad (8)$$

and

$$\tau_{mH} = \tau_{0H}\exp\left(\frac{E_H}{RT}\right), \quad (9)$$

where β_0 and β_Q are parameters representing the magnitude of distribution. They relate to the distributions of the pre-exponential factor and the activation energy centered by τ_{0H} and E_H, respectively. If $\beta_0 = 0$, only the activation energy has a distribution, which approach was applied to V–Nb–H and V–Ta–H(D) systems [22,23]. β_0 contributes to the distribution of the correlation time at all the temperature range, whereas β_Q contributes at low temperatures. f_1 is a correction factor which reduces only the effective M_{HV} [10,13]. The origin of the correction factor f_1 has never been elucidated, although the necessity was reported already in 1960s [24,25].

The T_1 data have been fitted by Eqs. (1) and (5) and the fitted curves are given in Figs. 6–9 by chain, solid and chain-dotted lines. M_{HH} and M_{HV} for $Ti_{0.33}V_{0.67}H_xD_y$ are $160x$ and 393 kHz^2, respectively, which are estimated from the crystal structures. The calculated total second moments ($= M_{HH} + M_{HV}$) are 537, 494, 471 and 449 kHz^2 for $Ti_{0.33}V_{0.67}H_{0.90}$, $Ti_{0.33}V_{0.67}H_{0.63}D_{0.29}$, $Ti_{0.33}V_{0.67}H_{0.49}D_{0.43}$ and $Ti_{0.33}V_{0.67}H_{0.35}D_{0.58}$, respectively. Those values are in fair agreement with the observed values, though the latter ones include large experimental errors. To reduce the number of the adjustable parameters, the τ_{0H} value is assumed to be 3×10^{-14} s for the T sites [6,7,12,13]. All the parameters obtained from the fitting procedure are listed in Table 3. The errors in the table are estimated on the base of the above assumptions. The estimated activation energy E_H is 21.3 kJ/mol, being independent of the [D]/[H] ratio. On the other hand, the distribution of the mean residence time decreases with the [D]/[H] ratio. Korringa constants are about 75 s K, and no clear dependence on the [D]/[H] ratio is obtained.

3.6. ^2H NMR spectra

^2H NMR spectra have been recorded for $Ti_{0.33}V_{0.67}H_xD_y$ at 30.7 and 61.4 MHz in the temperature range between 140 and 400 K. Fig. 10 shows ^2H NMR spectra at 61.4 MHz in $Ti_{0.33}V_{0.67}H_{0.49}D_{0.43}$, and other samples show similar spectra. Fine structures characteristic of quadrupole interaction are not observed, and the spreads of the signals are much narrower than those in VH_xD_y and $Ti_{0.1}V_{0.9}H_xD_y$ [7,14]. The narrow signal suggests that all the D atoms occupy the T sites, because the quadrupole interaction is smaller in the T sites than in the O sites. On the other hand, the ^2H spectra of VH_xD_y and $Ti_{0.1}V_{0.9}H_xD_y$ are composed of two components corresponding to the O and T sites [7,14].

The peak positions are –4 and –9 kHz from D_2O above 180 K and below 160 K, respectively. Some spectra show the presence of two peaks between 160 and 180 K, as shown by the spectrum at 175 K in Fig. 10. The temperature range of the spectral change does not agree with that of the DSC peaks and, therefore, the order–disorder transition is not concerned with the spectral change. There might be two components with their peak positions at –4 and –9 kHz. The –4-kHz component undergoes motional narrowing at 160–180 K, whereas the line shape of the –9-kHz component seems to be almost constant in the temperature range studied. Consequently, the –4-kHz and –9-kHz components are assigned to the monohydride and dihydride phases, respectively.

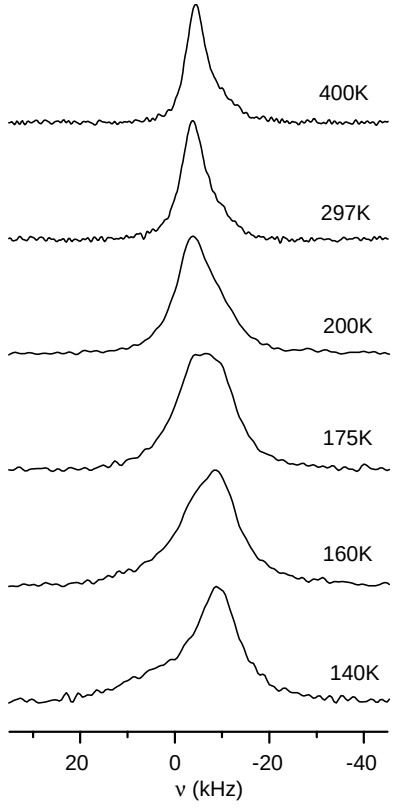

Fig. 10. Temperature dependence of ^2H NMR spectra in $Ti_{0.33}V_{0.67}H_{0.49}D_{0.43}$, measured at 61.4 MHz. The D_2O signal was set at the 0-Hz position.

3.7. ^2H spin-lattice relaxation time

^2H spin-lattice relaxation times, T_1, have been measured at 30.7 and 61.4 MHz in the temperature range between 140 and 400 K. The obtained T_1 values are plotted in Figs. 11–14. The experimental error of each T_1 value is $\pm 5\%$ or less. The T_1 values are determined by monitoring the peak height. Since the peak position changes in the temperature range between 160 and 180 K, the T_1 values change discontinuously in this temperature range. The apparent discontinuity of T_1 vs. $1000/T$ is due to the fact that the relaxation times are measured for the monohydride phase at high temperatures and for the dihydride phase at low temperatures. For the samples with the higher D contents, below 180 K the T_1 values for the –4-kHz component can be determined from the height of the shoulder at 61.4 MHz. In other cases, the relaxation curve for the shoulder position is largely affected by the –9-kHz component, and reliable T_1 values for the –4-kHz component are not available below 180 K.

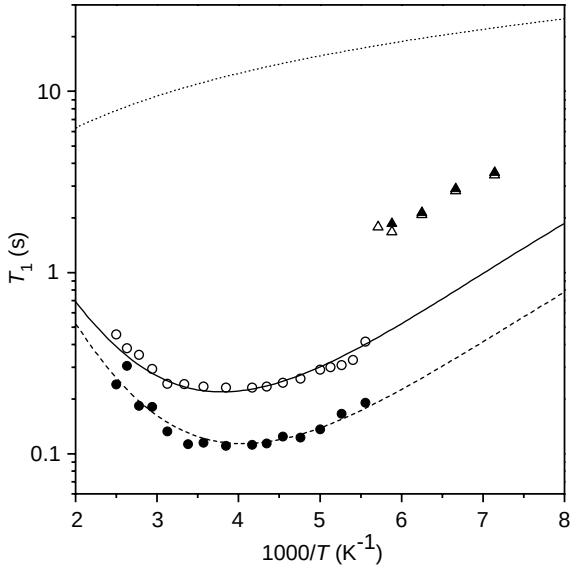

Fig. 11. ^2H spin-lattice relaxation times in $Ti_{0.33}V_{0.67}H_{0.63}D_{0.29}$ at 30.7 (●) and 61.4 MHz (○) for the –4-kHz component and at 30.7 (▲) and 61.4 kHz (△) for the –9-kHz component. Chain and solid lines are the simulated results and the dotted line indicates the contribution of conduction electrons.

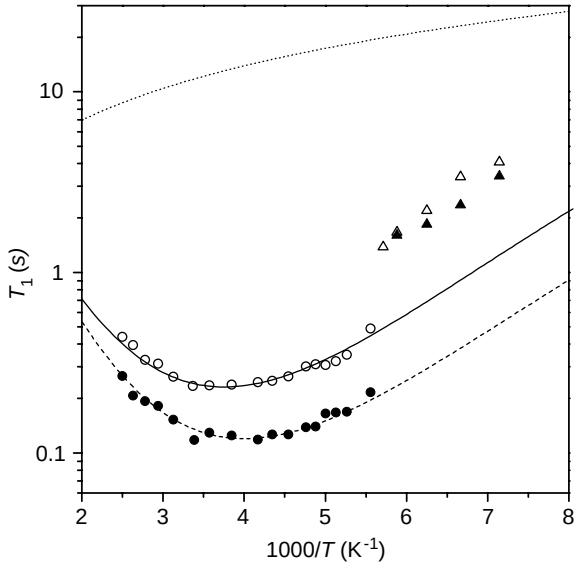

Fig. 12. ^{2}H spin-lattice relaxation times in $Ti_{0.33}V_{0.67}H_{0.49}D_{0.43}$ at 30.7 (●) and 61.4 MHz (○) for the –4-kHz component and at 30.7 (▲) and 61.4 kHz (△) for the –9-kHz component. Chain and solid lines are the simulated results and the dotted line indicates the contribution of conduction electrons.

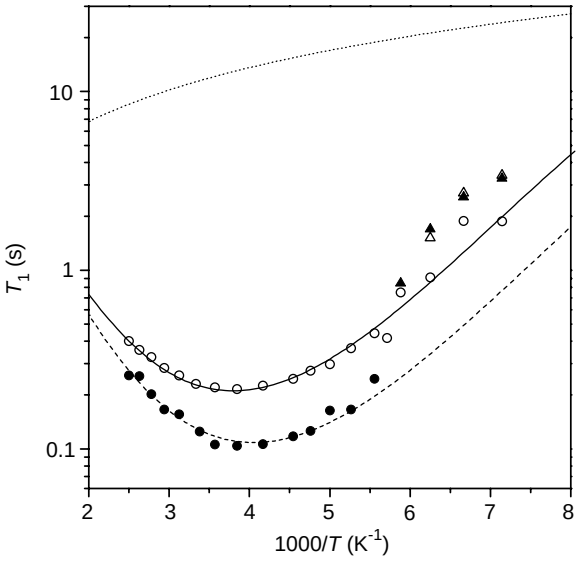

Fig. 13. ^{2}H spin-lattice relaxation times in $Ti_{0.33}V_{0.67}H_{0.35}D_{0.58}$ at 30.7 (●) and 61.4 MHz (○) for the –4-kHz component and at 30.7 (▲) and 61.4 kHz (△) for the –9-kHz component. Chain and solid lines are the simulated results and the dotted line indicates the contribution of conduction electrons.

The T_1 values for the –4-kHz component are dependent on Larmor frequency, while those for the –9-kHz component are independent of it. The relaxation mechanism of the latter component is not due to motions. Conduction electrons might contribute to the relaxation, but the –9-kHz component is out of the range of this work.

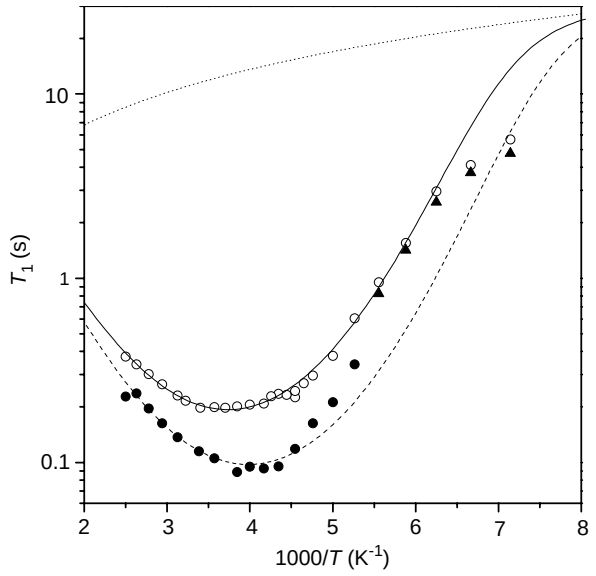

Fig. 14. ^{2}H spin-lattice relaxation times in $Ti_{0.33}V_{0.67}H_{0.07}D_{0.88}$ at 30.7 (●) and 61.4 MHz (○) for the –4-kHz component and at 30.7 MHz (▲) for the –9-kHz component. Chain and solid lines are the simulated results and the dotted line indicates the contribution of conduction electrons.

3.8. Analysis of ^{2}H spin-lattice relaxation time

The ^{2}H spin-lattice relaxation time in the present system is expressed as

$$(T_1)^{-1} = (T_{1d})^{-1} + (T_{1q})^{-1} + (T_{1e})^{-1} + (T_{1p})^{-1}, \quad (10)$$

where $(T_{1d})^{-1}$, $(T_{1e})^{-1}$ and $(T_{1p})^{-1}$ are the same as in Eq. (1), and $(T_{1q})^{-1}$ is contribution due to fluctuation of ^{2}H quadrupole interaction. ^{2}H Korringa constants $(T_{1e}T)$ are estimated from the respective ^{1}H Korringa constant multiplied by 42.44 $(=\gamma_H^2/\gamma_D^2)$, which are listed in Table 4. The ^{2}H Korringa constant for $Ti_{0.33}V_{0.67}H_{0.07}D_{0.88}$ is assumed to be the same as that of $Ti_{0.33}V_{0.67}H_{0.35}D_{0.58}$.

Because the dipolar relaxations in both ^{1}H and ^{2}H spins are dominated by the dipolar interaction with ^{51}V spins, the ratio of relaxation rates scales roughly γ_H^2/γ_D^2. The ^{1}H T_1 minimum values are 20–25 ms at 31.6 MHz and 40–50 ms at 60.0 MHz. The expected ^{2}H T_1 minimum values caused by the dipolar interaction are calculated as 0.8–1.1 s and 1.7–2.1 s at the corresponding frequencies. The experimental ^{2}H T_1 minimum values are 0.09–0.11 s and 0.2–0.24 s at 30.7 and 61.4 MHz, respectively. These comparisons between the scaled ^{1}H T_1 and the experimental ^{2}H T_1 show that the quadrupole interaction has an overwhelming effect in the ^{2}H spin-lattice relaxation.

Table 4
^{2}H Korringa constants and parameters of D diffusion

Sample	$T_{1e}T$[a] (s K)	Site	τ_{0D}[b] (s)	E_D[c] (kJ/mol)	β_Q[d] (kJ/mol)	β_0[e]	QCC[f] (kHz)
$Ti_{0.33}V_{0.67}H_{0.63}D_{0.29}$	3140	T	4.2×10^{-14}	22.0	7.0	3.5	34
$Ti_{0.33}V_{0.67}H_{0.49}D_{0.43}$	3480	T	4.2×10^{-14}	22.3	7.0	3.5	33
$Ti_{0.33}V_{0.67}H_{0.35}D_{0.58}$	3310	T	4.2×10^{-14}	22.5	5.2	3.5	33
$Ti_{0.33}V_{0.67}H_{0.07}D_{0.88}$	3310[g]	T	4.2×10^{-14}	23.5	0	3.5	32

[a] Estimated from ^{1}H Korringa constants.
[b] Assumed to be $1.4\tau_{0H}$.
[c] The error is about ±0.2.
[d] The error is about ±1.0.
[e] The error is about ±0.4.
[f] The error is about ±1.
[g] Assumed.

The BPP-type equation for the quadrupolar relaxation is described as [26]

$$(T_{1q})^{-1} = \frac{3}{40}\left(\frac{e^2Qq}{\hbar}\right)^2\left(1+\frac{\eta_Q^2}{3}\right) \times\left[\frac{\tau_D}{1+(\omega_D\tau_D)^2}+\frac{4\tau_D}{1+(2\omega_D\tau_D)^2}\right], \quad (11)$$

where ω_D and τ_D are an angular resonance frequency and a mean residence time of ^{2}H, respectively. e^2Qq/h (= QCC) is a quadrupole coupling constant and η_Q is an asymmetry factor. When the same type of distribution of the correlation time as that in ^{1}H T_1 is introduced, the $(T_{1q})^{-1}$ is described as

$$(T_{1q})^{-1} = \int F(S)\frac{3}{40}\left(\frac{e^2Qq}{\hbar}\right)^2\left(1+\frac{\eta_Q^2}{3}\right) \times\left[\frac{\tau_D}{1+(\omega_D\tau_D)^2}+\frac{4\tau_D}{1+(2\omega_D\tau_D)^2}\right] dS. \quad (12)$$

Relations similar to Eqs. (6)–(9) hold in ^{2}H also. The dipolar relaxation shows temperature and frequency dependences similar to those of the quadrupole relaxation. Only the quadrupole relaxation described by Eq. (12) is taken into account in the simulation. The asymmetry factor is set to zero. This is a good assumption for ^{2}H occupying the T sites, for which the electric-field-gradient tensor has approximately axial symmetry [7]. If there is a contribution from the dipolar interaction, the obtained parameter of the quadrupole coupling constant reflects its contribution.

The simulated results are shown in Figs. 11–14 by chain and solid lines. Similar to the ^{1}H T_1 analysis, the τ_{0D} values are assumed to be 4.2×10^{-14} s for the T sites from the relation that $\tau_{0D} = 1.4\tau_{0H}$ [6]. This relation is originated from the different masses of H and D. The obtained parameters are listed in Table 4. E_D increases slightly with the [D]/[H] ratio. On the other hand, the distribution of the mean residence time decreases with the [D]/[H] ratio. β_0 and β_Q are both necessary in this case. If either β_0 or β_Q is set to zero, the fitting is unsatisfactory, as shown in Fig. 15.

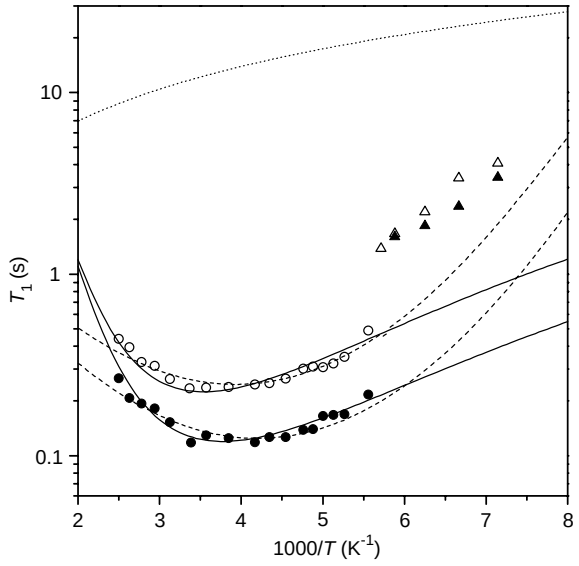

Fig. 15. Trial fittings for ^{2}H spin-lattice relaxation times in $Ti_{0.33}V_{0.67}H_{0.49}D_{0.43}$. Data are the same as in Fig. 12. Solid and chain lines are the simulated results assuming that $\beta_0 = 0$ and $\beta_Q = 11$ kJ/mol and that $\beta_0 = 5.5$ and $\beta_Q = 0$, respectively, with other parameters in Table 4 being unchanged. The dotted line indicates the contribution of conduction electrons.

3.9. Sites and dynamics of H and D

In the previous sections, we have analyzed the T_1 results by assuming the log-normal distribution of the correlation times as well as the pre-exponential factors in order to extract some trends in hydrogen diffusion. The obtained parameters listed in Tables 3 and 4 depend on the assumption, and thus the absolute values should be treated carefully. Several trends are extracted from a comparison between Tables 3 and 4, where the same type of analysis is applied to the T_1 results of both ^{1}H and ^{2}H.

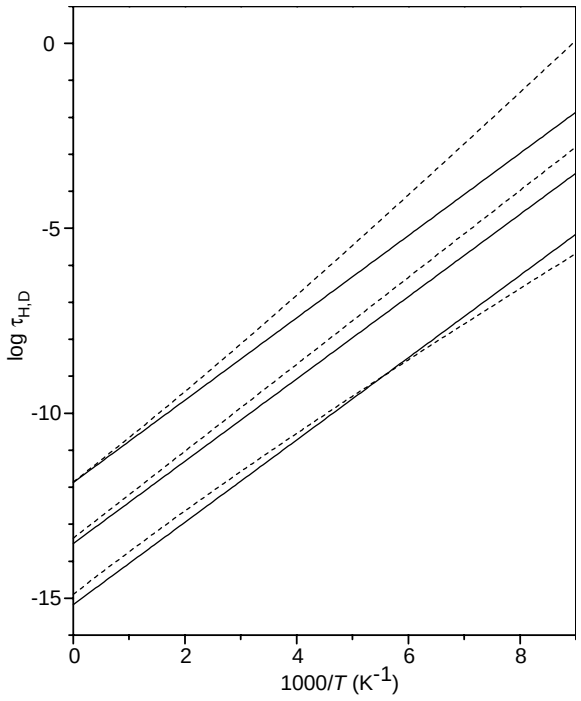

Fig. 16. The distribution of the mean residence times for $Ti_{0.33}V_{0.67}H_{0.49}D_{0.43}$. Solid and chain lines indicate the values of H and D, respectively. The three lines correspond to those at $S = +\beta_1, 0, -\beta_1$.

The $Ti_{0.33}V_{0.67}H_xD_y$ system has a bcc structure, and both H and D occupy the T sites. The mean activation energy is higher for the D diffusion than for the H diffusion (i.e., $E_H < E_D$). E_H is constant while E_D increases slightly with the [D]/[H] ratio. The distribution of the mean residence time decreases as the [D]/[H] ratio increases for both the H and D diffusions, and thus it is the smallest in the deuteride. In the temperature range studied (below 400 K) the distribution for the same sample is always larger in D than in H. For example, Fig. 16 shows the distribution of the mean residence times for $Ti_{0.33}V_{0.67}H_{0.49}D_{0.43}$.

The two-component nature of the ^1H NMR line shape reflects the distribution of the mean residence time. With increase in the D fraction the two-component nature becomes weak, which agrees the smaller distribution. The temperature range of the motional narrowing is in the order that $Ti_{0.33}V_{0.67}H_{0.90} < Ti_{0.33}V_{0.67}H_{0.63}D_{0.29} < Ti_{0.33}V_{0.67}H_{0.49}D_{0.43} < Ti_{0.33}V_{0.67}H_{0.35}D_{0.58}$. The narrow part of the spectra contributes largely to the ^1H FWHM and, thus, the FWHM decreases as the distribution increases. Consequently, the above order reflects the magnitude of the distribution.

The distribution of the mean residence time comes from the disorder in the metal arrangements as well as from neighboring hydrogen. Hydrogen is self-trapped by changing the positions of the surrounding metals slightly. This small displacement affects the energy potentials of the hydrogen sites nearby. The fact that the distribution of the mean residence time increases as the [H]/[D] ratio increases for both the H and D diffusions suggests that H makes a larger distribution in the surrounding H and D than D does. The result that the distribution is larger in D than in H suggests that D is disturbed more easily by the other H and D than H is. The local vibrational frequency of H is higher than that of D because of the different masses of H and D. Therefore, the zero-point vibrational energy of H is higher than that of D. This might be the origin of the difference in the distributions of H and D.

Further studies are needed to elucidate the origin of the difference in the distribution between ^1H and ^2H. The composition of the alloy also affects the distribution, and then the composition dependence is now being studied.

4. Conclusion

$Ti_{0.33}V_{0.67}$–H–D alloys with $([H]+[D])/([Ti]+[V]) \approx 0.9$ have been studied by means of XRD, DSC and ^1H and ^2H NMR, and the following conclusions have been obtained.

(1) The crystal structures of the monohydride phase are bcc at room temperature, although the lattice constants have a distribution.
(2) A phase transition similar to that from the δ_D phase to the α_D phase in the V–D system is observed in all the samples except for the protide, but the heat flow is very small.
(3) H and D occupy the T sites, and the parameters of hydrogen diffusion are estimated from the analysis of ^1H and ^2H T_1 by assuming a log-normal distribution of the correlation times as well as pre-exponential factors. The mean activation energy is higher for D diffusion than for H diffusion ($E_H < E_D$). E_H is constant while E_D increases slightly with the [D]/[H] ratio. The distribution of the mean residence time decreases for both H and D as the [D]/[H] ratio increases.

Acknowledgments

The author is grateful to Dr. E. Akiba of our institute for the primary hydrogenation. He also acknowledges the Central Research Laboratory of the Mitsubishi Metal Corporation for supplying the starting alloy. This study was financially supported by the Budget for Nuclear Research of the Ministry of Education, Culture, Sports, Science and Technology, based on the screening and counseling by the Atomic Energy Commission.

References

[1] H. Nagel, R.S. Perkins, Z. Metallkd. 66 (1975) 362.
[2] S. Ono, K. Nomura, Y. Ikeda, J. Less-Common Met. 72 (1980) 159.
[3] M. Hansen (Ed.), Constitution of Binary Alloys, 2nd Edition, McGraw-Hill, New York, 1958, p. 1241.
[4] S. Hayashi, K. Hayamizu, J. Less-Common Met. 161 (1990) 61.
[5] T. Ueda, S. Hayashi, Y. Nakai, S. Ikeda, Phys. Rev. B 51 (1995) 5725.
[6] T. Ueda, S. Hayashi, J. Alloys Compd. 256 (1997) 145.
[7] B. Bandyopadhyay, S. Hayashi, Phys. Rev. B 60 (1999) 10302.
[8] T. Schober, H. Wenzl, in: G. Alefeld, J. Völkl (Eds.), Hydrogen in Metals, Vol. II, Springer-Verlag, Berlin, 1978, p. 11.
[9] B. Nowak, M. Minier, J. Less-Common Met. 101 (1984) 245.
[10] S. Hayashi, K. Hayamizu, O. Yamamoto, J. Chem. Phys. 78 (1983) 5096.
[11] T. Ueda, S. Hayashi, K. Hayamizu, Phys. Rev. B 48 (1993) 5837.
[12] T. Ueda, S. Hayashi, J. Alloys Compd. 231 (1995) 226.
[13] B. Bandyopadhyay, S. Hayashi, J. Alloys Compd. 305 (2000) 136.
[14] B. Bandyopadhyay, S. Hayashi, J. Alloys Compd. 330–332 (2002) 443.
[15] S. Hayashi, Anal. Sci. 18 (2002) 599.
[16] S. Hayashi, K. Hayamizu, O. Yamamoto, J. Solid State Chem. 46 (1983) 306.
[17] N. Bloembergen, E.M. Purcell, R.V. Pound, Phys. Rev. 73 (1948) 679.
[18] T.C. Jones, T.K. Halstead, K.H.J. Buschow, J. Less-Common Met. 73 (1980) 209.
[19] T.K. Halstead, K. Metcalfe, T.C. Jones, J. Magn. Reson. 47 (1982) 292.
[20] Cl. Ritter, W. Muller-Warmuth, R. Schollhorn, J. Chem. Phys. 83 (1985) 6130.
[21] E.R. Andrew, D.J. Bryant, E.M. Cashell, Chem. Phys. Lett. 69 (1980) 551.
[22] L. Lichty, J. Shinar, R.G. Barnes, D.R. Torgeson, D.T. Peterson, Phys. Rev. Lett. 55 (1985) 2895.
[23] A.V. Skripov, M.Yu. Belyaev, A.P. Stepanov, L.N. Padurets, E.I. Sokolova, J. Alloys Compd. 190 (1993) 171.
[24] B. Pedersen, T. Krogdahl, O.E. Stokkeland, J. Chem. Phys. 42 (1965) 72.
[25] D. Rohy, R.M. Cotts, Phys. Rev. B 1 (1970) 2070.
[26] A. Abragam, The Principles of Nuclear Magnetism, Oxford University Press, London, 1961.